Asymmetric Laguerre-Gaussian beams

A. A. Kovalev, V. V. Kotlyar, and A. P. Porfirev
Laser Measurements laboratory, Image Processing Systems Institute, Samara 443001, Russia
and Technical Cybernetics Department, Samara State Aerospace University, Samara 443086, Russia
(Received 23 March 2016; published 28 June 2016)

We introduce a family of asymmetric Laguerre-Gaussian (aLG) laser beams. The beams have been derived via a complex-valued shift of conventional LG beams in the Cartesian plane. While propagating in a uniform medium, the first bright ring of the aLG beam becomes less asymmetric and the energy is redistributed toward peripheral diffraction rings. The projection of the orbital angular momentum (OAM) onto the optical axis is calculated. The OAM is shown to grow quadratically with increasing asymmetry parameter of the aLG beam, which equals the ratio of the shift to the waist radius. Conditions for the OAM becoming equal to the topological charge have been derived. For aLG beams with zero radial index, we have deduced an expression to define the intensity maximum coordinates and shown the crescent-shaped intensity pattern to rotate during propagation. Results of the experimental generation and rotation of aLG beams agree well with theoretical predictions.

DOI: 10.1103/PhysRevA.93.063858

I. INTRODUCTION

Laguerre-Gaussian (LG) modes comprise a well-studied class of light fields. The transverse intensity profile of these fields is invariant to the propagation in a uniform medium and shows a radial symmetry. The LG modes have found use in areas such as optical micromanipulation, quantum optics, and optical communications. Each mode of the class is characterized by two indices—radial and azimuthal, the latter defining the orbital angular momentum (OAM).

There is a long history and a considerable bulk of research dealing with LG modes, and articles concerned with the study of their properties [1–5], generation [6–8], and uses [9–14] have been actively published.

For instance, the propagation of composite vortex beams generated by coaxial superposition of LG beams with the identical location and size of the waist was discussed in [1]. Fields composed of equidistant arrays of solitary or tandem low-intensity spots located on diffractive rings have been generated. The physical meaning of the radial index of LG modes was looked into in [2], whereas [3] has studied in which way the three-dimensional intensity distribution of sharply focused LG beams depends on the homogeneous polarization (linear and circular) and topological charge. The polarization type was shown to have the greatest effect on the longitudinal E-field component, with the total intensity pattern showing the largest variations vs polarization when using the first-order vortex phase. The nonparaxial propagation of LG modes in the presence of an aperture was discussed in [4]. The diffraction by the aperture was shown to essentially distort the near-field pattern, while having an unessential effect on the far-field intensity (unless the aperture blocked off a substantial proportion of the beam). Properties of light fields that carried the OAM, had no radial symmetry, and were affected by a harmonic potential were analyzed in [5]. A technique for generating LG modes in a cavity of a solid-state laser was proposed in [6]. Generation of lower-order LG modes with the ability to control the topological charge by means of a solid-state laser was discussed in [7]. LG modes with nonzero radial index were generated by means of spiral zone plates in [8]. In [9] an operator was considered which was linked with the radial index in the Laguerre-Gauss modes of a two-dimensional harmonic oscillator in cylindrical coordinates. In [10], the replacement of a conventional Gaussian beam with a LG beam was shown to result in a reduced Doppler width in the absorption spectrum of ^{85}Rb and ^{87}Rb atoms. The reduction of the thermal noise effect on gravitational wave detectors with use of the LG modes was discussed in [11]. Spin-orbital coupling of ultracold atoms with the aid of LG beams was reported in [12]. The interaction of a LG beam with an atom or a diatomic molecule was studied in [13]. The transfer of the orbital angular momentum between the mass center and internal motion of a sufficiently cooled atom or molecule has been shown to take place. A three-dimensional off-axis optical trap for dielectric submicron microbeads created with a single LG beam was described in [14]. The classical communication by means of LG modes at a 3-km distance in a turbulent atmosphere was demonstrated in [15]. The quantum communication with entangled twisted photons was described in [16]. Note that in addition to laser beams, electron beams [17] and even neutron beams [18] can carry the OAM.

The above review of the latest publications relating to LG beams suggests that not only do they find new applications but also form a basis for constructing advanced light fields that have been studied theoretically so far. Alongside looking into the properties of various superpositions of the familiar laser beams, it is possible to obtain novel beams of interest by simply performing a complex-valued shift of their complex amplitude in the Cartesian plane. It is known that if a paraxial point source is shifted along the optical axis by an imaginary distance, then instead of a parabolic wave, a Gaussian beam is generated [19]. Asymmetric diffraction-free Bessel modes that produce a crescent-shaped transverse intensity pattern have been generated in a similar way [20]. However, Bessel beams have infinite energy and therefore can be physically realized only approximately. In addition, the dependence of the OAM on the asymmetry parameter is linear for Bessel beams [20], while for the asymmetric Laguerre-Gaussian beams under study this dependence is parabolic.

In this work, also making use of a complex-valued shift in the Cartesian plane, we conduct theoretical and experimental studies of asymmetric Laguerre-Gaussian (aLG) beams. As in

conventional LG beams—and as distinct from Bessel beams—their transverse intensity pattern consists of a finite number of diffraction rings, which, however, have a nonuniform intensity distribution. As the aLG mode propagates in a uniform medium, the intensity of the peripheral ring increases. The OAM and power of the aLG beam is calculated analytically. In particular, we analyze aLG beams with zero radial index that have a crescent-shaped transverse intensity pattern. For such beams, an analytic relation for the coordinates of the intensity peak is derived and the diffraction pattern is shown to rotate upon propagation in a uniform medium. An aLG beam with zero radial index is generated using a spatial light modulator and experimentally shown to rotate in space during propagation. A feasibility to generate the superposition of misaligned beams that has a near-Gaussian intensity pattern and rotates as a whole during propagation in space is demonstrated.

Elliptical beams [21] have been known to constitute the most general family of paraxial laser beams. Circular beams [22] and Ince-Gaussian beams [23] are partial cases of the elliptical beams. At definite parameters these beams carry a nonzero OAM, but these beams cannot be reduced to LG modes, nor to elegant or asymmetric LG beams. In addition, the Ince polynomials do not have a closed form, making it difficult to derive analytical expressions for them. For example, a closed expression for the OAM of an elliptical vortex [21] cannot be obtained.

II. ASYMMETRIC LAGUERRE-GAUSSIAN BEAMS

The complex amplitude of a conventional LG beam in polar coordinates in the initial plane is given by [24]

$$E_{mn}(r,\varphi,z=0)=\left(\frac{\sqrt{2}r}{w_0}\right)^n L_m^n\left(\frac{2r^2}{w_0^2}\right)\exp\left(-\frac{r^2}{w_0^2}+in\varphi\right), \tag{1}$$

where (r, φ, z) are cylindrical coordinates, w_0 is the Gaussian beam waist, n is the topological charge of an optical vortex, and $L_m^n(x)$ is an adjoint Laguerre polynomial.

If the beam is shifted by x_0 along the x coordinate and by y_0 along the y coordinate (x_0 and y_0 can take complex values), the beam amplitude in the Cartesian coordinates takes the form

$$E_{mn}(x,y,z=0)=\left(\frac{\sqrt{2}}{w_0}\right)^n[(x-x_0)+i(y-y_0)]^n \times\exp\left(-\frac{s^2}{w_0^2}\right)L_m^n\left(\frac{2s^2}{w_0^2}\right), \tag{2}$$

where $s^2=(x-x_0)^2+(y-y_0)^2$.

When propagating in free space at an arbitrary distance z, the beam complex amplitude takes the form

$$E_{mn}(x,y,z)=\frac{w(0)}{w(z)}\left[\frac{\sqrt{2}}{w(z)}\right]^n[(x-x_0)+i(y-y_0)]^n \times L_m^n\left[\frac{2s^2}{w^2(z)}\right]\exp\left[-\frac{s^2}{w^2(z)}+\frac{iks^2}{2R(z)} -i(n+2m+1)\zeta(z)\right], \tag{3}$$

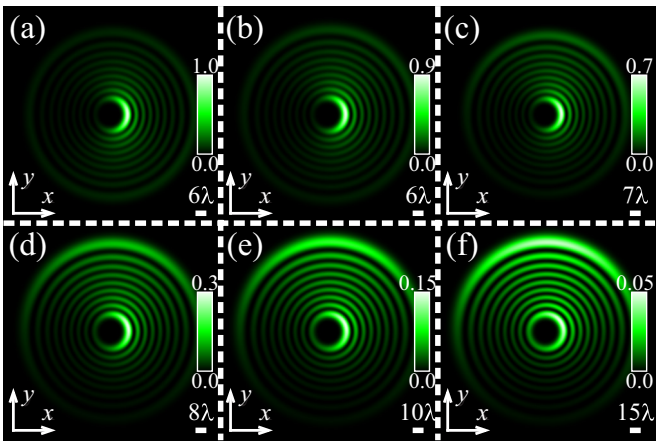

FIG. 1. The transverse intensity pattern of an aLG beam in different planes for the parameters: wavelength $\lambda = 532$ nm, waist radius $w_0 = 10\lambda$, beam index $(m, n) = (8, 7)$, transverse shifts $x_0 = 0$ and $y_0 = i\lambda$; the on-axis distances are $z = 0\lambda$ (a), $z = z_R/4 = 25\pi\lambda$ (b), $z = z_R/2 = 50\pi\lambda$ (c), $z = z_R = 100\pi\lambda$ (d), $z = 3z_R/2 = 150\pi\lambda$ (e), and $z = 5z_R/2 = 250\pi\lambda$ (f).

where

$$w(z)=w_0\sqrt{1+\left(\frac{z}{z_R}\right)^2},\quad R(z)=z\left[1+\left(\frac{z_R}{z}\right)^2\right],\quad \zeta(z)=\arctan\left(\frac{z}{z_R}\right). \tag{4}$$

$z_R = kw_0^2/2$ is the Rayleigh range and $k = 2\pi/\lambda$ is the wave number of light of wavelength λ.

If the shifts x_0 and y_0 are not real valued, then the magnitudes s^2, $w(z)$, and $R(z)$ do not have the same physical meaning as for real x_0 and y_0, no more, respectively, denoting a distance from the optical axis, a beam width, and a wavefront curvature radius. Besides, unlike conventional LG beams, the transverse intensity pattern of such a beam is not radially symmetric. Figure 1 depicts simulated intensity patterns of beam (3) at different distances for the following values of parameters: wavelength, $\lambda = 532$ nm; waist radius, $w_0 = 10\lambda$; beam index $(m, n) = (8, 7)$; transverse shifts $x_0 = 0$, $y_0 = i\lambda$; and the on-axis distances are $z = 0\lambda$ [Fig. 1(a)], $z = z_R/4 = 25\pi\lambda$ [Fig. 1(b)], $z = z_R/2 = 50\pi\lambda$ [Fig. 1(c)], $z = z_R = 100\pi\lambda$ [Fig. 1(d)], $z = 3z_R/2 = 150\pi\lambda$ [Fig. 1(e)], and $z = 5z_R/2 = 250\pi\lambda$ [Fig. 1(f)]. The computational domain size is $2R$, where $R = 60\lambda$ [Figs. 1(a) and 1(b)], 70λ [Fig. 1(c)], 80λ [Fig. 1(d)], 100λ [Fig. 1(e)], and 150λ [Fig. 1(f)]. At the above parameters, the Rayleigh range is $z_R = 100\pi\lambda$.

Figure 1 suggests that upon propagation the first crescent-shaped ring nearly turns into a ring, although this is not the case for the peripheral rings. As the aLG beam propagates, the energy is also seen to be redistributed from the central to peripheral crescents.

III. POWER OF A SHIFTED LAGUERRE-GAUSSIAN BEAM

The power of a paraxial light beam can be expressed through both the complex amplitude E and the angular spectrum of plane waves, A:

$$W = \int_{-\infty}^{-\infty}\int_{-\infty}^{+\infty} E^* E dx dy = \lambda^2 \int_{-\infty}^{-\infty}\int_{-\infty}^{+\infty} A^* A d\alpha d\beta, \tag{5}$$

where

$$A(\alpha,\beta) = \lambda^{-2}\int_{-\infty}^{+\infty}\int_{-\infty}^{+\infty} E(x,y,0) \times \exp[-ik(\alpha x+\beta y)]dxdy. \tag{6}$$

For an aLG beam, the power can be more conveniently calculated in the spectral plane. First, we derive a relation for the angular spectrum of a nonshifted beam:

$$\begin{aligned} A(\rho,\theta) &= \frac{1}{\lambda^2}\left(\frac{\sqrt{2}}{w_0}\right)^n \int_0^\infty r^n \exp\left(-\frac{r^2}{w_0^2}\right) L_m^n\left(\frac{2r^2}{w_0^2}\right) \\ &\quad\times\left\{\int_0^{2\pi} \exp\left[in\varphi - ik\rho r\cos(\varphi-\theta)\right]d\varphi\right\} r dr \\ &= (-i)^n \frac{k^2}{2\pi}\left(\frac{\sqrt{2}}{w_0}\right)^n \exp(in\theta) \\ &\quad\times\int_0^\infty r^{n+1}\exp\left(-\frac{r^2}{w_0^2}\right) L_m^n\left(\frac{2r^2}{w_0^2}\right) J_n(k\rho r)dr, \end{aligned} \tag{7}$$

where (r,φ) and (ρ,θ) are polar coordinates in the initial plane and in the Fourier plane, respectively (ρ is a dimensionless coordinate).

We shall make use of a reference integral ([25], Eq. 7.421.4):

$$\begin{aligned} &\int_0^\infty x^{\nu+1}\exp(-\beta x^2) L_n^\nu(\alpha x^2) J_\nu(xy)dx \\ &\quad= \frac{(\beta-\alpha)^n y^\nu}{2^{\nu+1}\beta^{\nu+n+1}}\exp\left(-\frac{y^2}{4\beta}\right) L_n^\nu\left[\frac{\alpha y^2}{4\beta(\alpha-\beta)}\right]. \end{aligned} \tag{8}$$

In view of (8), the angular spectrum of plane waves of a LG beam is

$$A(\rho,\theta) = C_0\rho^n L_m^n\left[\frac{(kw_0\rho)^2}{2}\right]\exp\left[-\frac{(kw_0\rho)^2}{4}+in\theta\right], \tag{9}$$

where

$$C_0 = (-i)^n(-1)^m\frac{(kw_0)^{n+2}}{2^{2+n/2}\pi}. \tag{10}$$

For the shifted beam in Eq. (2), the angular spectrum of the plane waves takes the form

$$\begin{aligned} A(\rho,\theta) &= C_0\rho^n\exp\left[-\frac{(kw_0\rho)^2}{4}+in\theta\right] \\ &\quad\times L_m^n\left[\frac{(kw_0\rho)^2}{2}\right]\exp\left[-ik\rho(x_0\cos\theta+y_0\sin\theta)\right]. \end{aligned} \tag{11}$$

Making use of Eq. (11), the power of the aLG beam is given by

$$\begin{aligned} W &= 2\pi\lambda^2|C_0|^2\int_0^\infty \rho^{2n+1}\exp\left[-\frac{(kw_0\rho)^2}{2}\right] \\ &\quad\times\left\{L_m^n\left[\frac{(kw_0\rho)^2}{2}\right]\right\}^2 J_0(2ikD_0\rho)d\rho, \end{aligned} \tag{12}$$

where $D_0 = [(\mathrm{Im}x_0)^2 + (\mathrm{Im}y_0)^2]^{1/2}$.

Integral (12) can be calculated using a reference integral (Eq. 2.9.12.14 in [26]), which, following a numerical checkup, reads as

$$\begin{aligned} &\int_0^\infty x^{(\gamma+\delta)/2}e^{-cx}J_{\gamma+\delta}(b\sqrt{x})L_\mu^\gamma(cx)L_\nu^\delta(cx)dx \\ &\quad= \frac{(-1)^{\mu+\nu}}{c^{\gamma+\delta+1}}\left(\frac{b}{2}\right)^{\gamma+\delta}\exp\left(-\frac{b^2}{4c}\right) \\ &\quad\times L_\nu^{\gamma+\mu-\nu}\left(\frac{b^2}{4c}\right)L_\mu^{\delta-\mu+\nu}\left(\frac{b^2}{4c}\right), \end{aligned} \tag{13}$$

where $\mathrm{Re}c > 0, \mathrm{Re}(\gamma+\delta) > -1, |\arg b| < \pi$. In (13), we change the integration variable $x \to x^2$ and set $\mu = m, \gamma = n, \delta = -n, \nu = m+n, c = (kw_0)^2/2$, and $b = 2ikD_0$. Then, considering the identity

$$L_\mu^{-\sigma}(x) \equiv [(\mu-\sigma)!/\mu!](-x)^\sigma L_{\mu-\sigma}^\sigma(x),$$

we obtain the beam power:

$$\begin{aligned} W &= \frac{\pi w_0^2}{2}\frac{(m+n)!}{m!}\times\exp\left(\frac{2D_0^2}{w_0^2}\right)L_{m+n}^0 \\ &\quad\times\left(-\frac{2D_0^2}{w_0^2}\right)L_m^0\left(-\frac{2D_0^2}{w_0^2}\right). \end{aligned} \tag{14}$$

Although being proportional to the Laguerre polynomials, the beam power cannot take negative or zero values. The reason is that $2(D_0/w_0)^2 \geqslant 0$, whereas the Laguerre polynomials are always positive in the nonpositive domain:

$$\begin{aligned} L_m(-\xi) &= \sum_{k=0}^m \frac{(-1)^k}{k!}C_m^k(-\xi)^k = \sum_{k=0}^m C_m^k\frac{\xi^k}{k!} \\ &= 1 + \underbrace{\sum_{k=1}^m C_m^k\frac{\xi^k}{k!}}_{\geqslant 0} \geqslant 1, \end{aligned} \tag{15}$$

where C_m^k are binomial coefficients.

From (15) and the presence of the factor $\exp[2(D_0/w_0)^2]$ in (14), we can infer that a complex-valued shift always results in an increased power of the beam.

In a particular case, when the beam is shifted by a real distance, the parameter D_0 takes a zero value and the power equals $[\pi w_0^2/2][(m+n)!/m!]$, which is coincident with the power of LG beams reported in [24] within a constant.

The increase in the power of the aLG beam with increasing asymmetry has no physical meaning. However, we shall use Eq. (14) in Sec. IV to calculate the normalized OAM.

IV. ORBITAL ANGULAR MOMENTUM OF A SHIFTED LAGUERRE-GAUSSIAN BEAM

Let us derive a relation for the projection of the OAM of an aLG beam on the optical axis. Note that the rest of the projections of a paraxial beam equal zero. This is also convenient to do using the angular spectrum of plane waves:

$$J_z = -i\lambda^2 \int_0^\infty \int_0^{2\pi} A^* \frac{\partial A}{\partial \theta} \rho d\rho d\theta. \tag{16}$$

Substituting (11) in (16) yields

$$J_z = -i\lambda^2 |C_0|^2 \int_0^\infty \int_0^{2\pi} \rho^{2n} \exp\left[-\frac{(kw\rho)^2}{2}\right] \left\{L_m^n\left[\frac{(kw\rho)^2}{2}\right]\right\}^2 \exp[-in\theta + ik\rho(x_0^* \cos\theta + y_0^* \sin\theta)]$$
$$\times [in + ik\rho(x_0 \sin\theta - y_0 \cos\theta)] \exp[in\theta - ik\rho(x_0 \cos\theta + y_0 \sin\theta)] \rho d\rho d\theta. \tag{17}$$

We can single out a term proportional to the power:

$$J_z = nW + k\lambda^2 |C_0|^2 \int_0^\infty \rho^{2n+2} \exp\left[-\frac{(kw\rho)^2}{2}\right] \left\{L_m^n\left[\frac{(kw\rho)^2}{2}\right]\right\}^2 d\rho \int_0^{2\pi} (x_0 \sin\theta - y_0 \cos\theta)$$
$$\times \exp\{2k\rho[(\mathrm{Im}x_0)\cos\theta + (\mathrm{Im}y_0)\sin\theta]\} d\theta. \tag{18}$$

The inner integral is expressed through Bessel functions [27]. Then, (18) takes the form

$$J_z = nW - 2\pi k\lambda^2 |C_0|^2 \int_0^\infty \rho^{2n+2} \exp\left[-\frac{(kw\rho)^2}{2}\right] \left\{L_m^n\left[\frac{(kw\rho)^2}{2}\right]\right\}^2$$
$$\times \left\{(ix_0 + y_0)\left[\frac{(\mathrm{Im}x_0) - (\mathrm{Im}y_0)}{2iD_0}\right] + (ix_0 - y_0)\left[\frac{(\mathrm{Im}x_0) - (\mathrm{Im}y_0)}{2iD_0}\right]^{-1}\right\} i I_1(2kD_0\rho) d\rho$$
$$= nW + 4\pi^2 \lambda |C_0|^2 \frac{\mathrm{Im}(x_0^* y_0)}{D_0} \int_0^\infty \rho^{2n+2} \exp\left[-\frac{(kw\rho)^2}{2}\right] \left\{L_m^n\left[\frac{(kw\rho)^2}{2}\right]\right\}^2 I_1(2kD_0\rho) d\rho. \tag{19}$$

The integral in (19) can be calculated in a way similar to the beam power integral by expressing it as a derivative with respect to D_0:

$$J_z = nW - 4\pi^2 \lambda |C_0|^2 \frac{\mathrm{Im}(x_0^* y_0)}{2kD_0} \frac{\partial}{\partial D_0} \left(\int_0^\infty \rho^{2n+1} \exp\left[-\frac{(kw\rho)^2}{2}\right] \left\{L_m^n\left[\frac{(kw\rho)^2}{2}\right]\right\}^2 I_0(2kD_0\rho) d\rho \right). \tag{20}$$

The integral in (20) can be taken, being coincident with the power integral:

$$J_z = nW - 4\pi^2 \lambda |C_0|^2 \frac{\mathrm{Im}(x_0^* y_0)}{2kD_0} \frac{\partial}{\partial D_0} \left\{ \frac{2^n}{(kw_0)^{2n+2}} \frac{(m+n)!}{m!} \exp\left(\frac{2D_0^2}{w_0^2}\right) L_{m+n}\left(-\frac{2D_0^2}{w_0^2}\right) L_m\left(-\frac{2D_0^2}{w_0^2}\right) \right\}$$
$$= nW - \frac{\pi w_0^2}{4} \frac{(m+n)!}{m!} \frac{\mathrm{Im}(x_0^* y_0)}{D_0} \frac{\partial}{\partial D_0} \left\{ \exp\left(\frac{2D_0^2}{w_0^2}\right) L_{m+n}\left(-\frac{2D_0^2}{w_0^2}\right) L_m\left(-\frac{2D_0^2}{w_0^2}\right) \right\}. \tag{21}$$

After taking the derivative, the normalized OAM takes the form

$$\frac{J_z}{W} = n + \frac{2\mathrm{Im}(x_0^* y_0)}{w_0^2} \left[\frac{L_m^1\left(-\frac{2D_0^2}{w_0^2}\right)}{L_m\left(-\frac{2D_0^2}{w_0^2}\right)} + \frac{L_{m+n}^1\left(-\frac{2D_0^2}{w_0^2}\right)}{L_{m+n}\left(-\frac{2D_0^2}{w_0^2}\right)} - 1 \right]. \tag{22}$$

The physical meaning of the second term on the right-hand side of Eq. (22) can be better understood at $n = m = 0$. In this case, the laser beam transforms into an asymmetric Gaussian beam. The first term in Eq. (22) is equal to zero ($n = 0$), while the second one reads as $4\mathrm{Im}(x_0^* y_0)/w_0^2$. It means that if the shift of the Gaussian beam is real (i.e., $x_0 = y_0 = aw_0$), then the Gaussian beam is just displaced and not deformed; i.e., $J_z/W = 0$. If both shifts are purely imaginary along both coordinates (i.e., $x_0 = y_0 = iaw_0$), then the shape of the Gaussian beam is distorted, while we still have $J_z/W = 0$. Only when the shift is real along one coordinate and imaginary along the other (i.e., $ix_0 = y_0 = iaw_0$), is the Gaussian beam then displaced, with its shape being distorted and it acquiring the OAM: $J_z/W = 4a^2$. This is also true for the aLG-beam at any other values of n and m.

From (22), the normalized OAM is seen to be independent of the wavelength and fully defined by the ratio of the shifts to the waist radius, i.e., by x_0/w_0 and y_0/w_0.

The increase or decrease of the normalized OAM can be shown to be fully determined by the sign of the magnitude $\mathrm{Im}(x_0^* y_0)$, because the expression in the square brackets in (22) is always larger than or equal to 1.

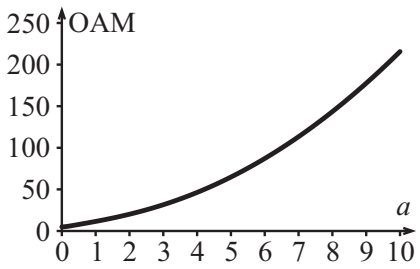

FIG. 2. Normalized OAM vs normalized asymmetry parameter $a(n = 5)$.

The normalized OAM depends simultaneously on several parameters, namely, two indices of the Laguerre polynomial and the real and imaginary shifts in the Cartesian coordinates. Let us analyze a particular case of purely imaginary magnitude $x_0^* y_0$, whereas the complex shifts have the same absolute value. Let $x_0 = a w_0 \exp(i\upsilon)$, $y_0 = i x_0$, where a is a real number (i.e., $a = |x_0/w_0|$). Then, the normalized OAM is given by

$$\frac{J_z}{W} = n - \xi\left[\frac{L_m^1(\xi)}{L_m(\xi)} + \frac{L_{m+n}^1(\xi)}{L_{m+n}(\xi)} - 1\right], \tag{23}$$

where $\xi = -2a^2$. The a parameter can be referred to as an asymmetry parameter of the aLG beam. Equation (23) suggests that at $|\xi| \gg 1$ the normalized OAM approximately equals $J_z/W \approx n - \xi$, depending quadratically on the asymmetry parameter a, as is confirmed by the graph in Fig. 2 plotted using Eq. (23) for $m = 3$ and $n = 5$.

From Fig. 2 it is seen that as distinct from conventional LG beams, the OAM of aLG beams varies in a continuous manner, taking integer and fractional values.

From (22) it follows that if $x_0^* y_0$ is a real number, in a similar way to radially symmetric optical vortices, the normalized OAM is coincident with the topological charge n, although the beam has no radial symmetry (if x_0 and y_0 are purely imaginary). Thus, Fig. 3 depicts intensity patterns

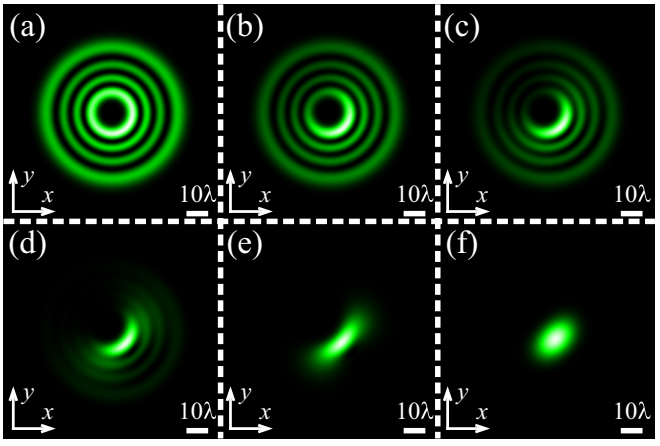

FIG. 3. Intensity patterns in the plane $z = 0$ for the aLG beams at the following parameters: wavelength $\lambda = 532$ nm, waist radius $w = 10\lambda$, beam index $(m, n) = (3, 5)$; at transverse shifts $x_0 = 0.01wi$ and $y_0 = 0.01wi$(a), $x_0 = 0.05wi$ and $y_0 = 0.05wi$(b), $x_0 = 0.1wi$ and $y_0 = 0.1wi$(c), $x_0 = 0.2wi$ and $y_0 = 0.2wi$ (d), $x_0 = 0.5wi$ and $y_0 = 0.5wi$(e), and $x_0 = 2wi$ and $y_0 = 2wi$(f).

in the plane $z = 0$ for the aLG beams with the following parameters: wavelength $\lambda = 532$ nm, waist radius $w = 10\lambda$, beam index $(m, n) = (3, 5)$, transverse shifts $x_0 = i0.01w$ and $y_0 = i0.01w$ [Fig. 3(a)], $x_0 = 0.05wi$ and $y_0 = 0.05wi$ [Fig. 3(b)], $x_0 = 0.1wi$ and $y_0 = 0.1wi$ [Fig. 3(c)], $x_0 = 0.2wi$ and $y_0 = 0.2wi$ [Fig. 3(d)], $x_0 = 0.5wi$ and $y_0 = 0.5wi$ [Fig. 3(e)], and $x_0 = 2wi$ and $y_0 = 2wi$ [Fig. 3(f)]. The computational domain size is $2R$, where $R = 50\lambda$. Equation (22) suggests that in all pictures in Fig. 3, the OAM should be equal to 5. From the numerical simulation, the OAM was found to equal 4.999 [Figs. 3(a) and 3(d)] and 4.998 [Figs. 3(e) and 3(f)].

All the beams in Fig. 3 are seen to be different in shape, showing near-radially symmetric diffraction rings in Fig. 3(a), an intensity crescent enclosed by peripheral rings in Figs. 3(b) and 3(c), a crescent with disintegrated peripheral rings in Fig. 3(d), a crescent with no peripheral rings in Fig. 3(e), and an elliptic intensity spot in Fig. 3(f). However, despite being different in shape, all these beams have the same OAM.

Note that although the beam in Fig. 3(f) looks like an elliptical Gaussian beam, this beam has the index $(m, n) = (3, 5)$ and its OAM equals 5. For the explanation of the shape of the beam in Fig. 3(f) we use Eq. (11). From Eq. (11) it follows that for purely imaginary large shifts along both coordinates ($x_0 = y_0 = 2wi$), the second exponent in Eq. (11) grows the fastest with increasing ρ at $\theta = \pi/4$. Thus, only a proportion of the spectrum in (11) in the first quadrant near the angle $\theta = \pi/4$ gives an effective contribution to the field of Eq. (3). Therefore, the field (3) is effectively generated only in the fourth quadrant with its center positioned at the angle $\varphi = -\pi/4$. Since only a small proportion of spectrum (11) contributes to field (3), there are no narrow bright rings in Fig. 3(f) that are seen in Fig. 3(a).

V. PARAXIAL LAGUERRE-GAUSSIAN BEAMS IN THE FORM OF A ROTATING CRESCENT

Equation (3) is essentially simplified at $m = 0$, with the diffraction pattern having a single ring. Then, the intensity takes the form

$$\begin{aligned} I_{0n}(x,y,z) &= |E|^2 = \frac{w^2(0)}{w^2(z)}\left[\frac{\sqrt{2}}{w^2(z)}\right]^n \exp\left[2\frac{(\mathrm{Im}x_0)^2 + (\mathrm{Im}y_0)^2}{w^2(z)}\right] \\ &\times [(u + \mathrm{Im}y_0)^2 + (v - \mathrm{Im}x_0)^2]^n \\ &\times \exp\left\{-\frac{2(u^2+v^2)}{w^2(z)} + \frac{2k[(\mathrm{Im}x_0)u + (\mathrm{Im}y_0)v]}{R(z)}\right\}, \end{aligned} \tag{24}$$

where $u = x - \mathrm{Re}x_0$, $v = y - \mathrm{Re}y_0$.

Considering that the intensity cannot be negative, the intensity zeros are its minima. From (24) it is seen that as the aLG beam propagates in a uniform space at $n > 0$, the central intensity minimum is observed at the point $(x_{\min}, y_{\min}) = (\mathrm{Re}x_0 - \mathrm{Im}y_0, \mathrm{Re}y_0 + \mathrm{Im}x_0)$, forming a phase singularity. Setting the partial Cartesian derivatives of intensity (24) equal to zero, we can show that at $n > 0$ the location of the intensity peak is a function of the distance z traveled and

rotates about the minimum:

$$\frac{y_{\max}-\mathrm{Re}y_0-\mathrm{Im}x_0}{x_{\max}-\mathrm{Re}x_0+\mathrm{Im}y_0}=\frac{(\mathrm{Im}y_0)z-(\mathrm{Im}x_0)z_R}{(\mathrm{Im}x_0)z+(\mathrm{Im}y_0)z_R}, \tag{25}$$

where $(x_{\max}, y_{\max})$ are the coordinates of the maximum intensity point.

Let us introduce a new coordinate system which is shifted and rotated around the initial system by an angle defined by the distance traveled, z:

$$\begin{pmatrix}\xi\\ \eta\end{pmatrix}=\begin{pmatrix}\cos\varphi & \sin\varphi\\ -\sin\varphi & \cos\varphi\end{pmatrix}\begin{pmatrix}x-\mathrm{Re}x_0+\mathrm{Im}y_0\\ y-\mathrm{Re}y_0-\mathrm{Im}x_0\end{pmatrix}, \tag{26}$$

where

$$\begin{aligned}\varphi&=\arctan\left[\frac{(\mathrm{Im}y_0)z-(\mathrm{Im}x_0)z_R}{(\mathrm{Im}x_0)z+(\mathrm{Im}y_0)z_R}\right],\\ \cos\varphi&=\frac{(\mathrm{Im}x_0)z+(\mathrm{Im}y_0)z_R}{D_0\sqrt{z^2+z_R^2}},\\ \sin\varphi&=\frac{(\mathrm{Im}y_0)z-(\mathrm{Im}x_0)z_R}{D_0\sqrt{z^2+z_R^2}}.\end{aligned} \tag{27}$$

It follows from Eq. (27), that if $\mathrm{Im}(y_0)=\mathrm{Im}(x_0)$, then in the initial plane ($z=0$) the light crescent is rotated by the angle $-\pi/4$, which is confirmed by Fig. 3.

In the new coordinate system (ξ,η), intensity (24) takes the form

$$I_{0n}(\xi,\eta,z)=|E|^2=\frac{w^2(0)}{w^2(z)}\left[\frac{\sqrt{2}}{w^2(z)}\right]^n(\xi^2+\eta^2)^n \times\exp\left[-\frac{2(\xi^2+\eta^2)}{w^2(z)}+\frac{2kD_0}{\sqrt{z^2+z_R^2}}\xi\right]. \tag{28}$$

Such a function can be shown to have three stationary points. The first point is a minimum at $\xi=0,\eta=0$, which corresponds to the above-mentioned point $(x_{\min}, y_{\min})$. The second point is a maximum with the coordinates

$$\begin{cases}\xi_{\max}=\dfrac{1}{2}\dfrac{w(z)}{w(0)}\left(D_0+\sqrt{D_0^2+2nw_0^2}\right)\\ \eta_{\max}=0\end{cases}, \tag{29}$$

and the third one is a saddle point with the coordinates

$$\begin{cases}\xi_{\mathrm{saddle}}=\dfrac{1}{2}\dfrac{w(z)}{w(0)}\left(D_0-\sqrt{D_0^2+2nw_0^2}\right)\\ \eta_{\mathrm{saddle}}=0\end{cases}, \tag{30}$$

where there is an intensity maximum with respect to the variable ξ and a minimum with respect to the variable η. The intensity maximum with respect to ξ means that the point is found on a bright ring, whereas the minimum with respect to η is where the minimal intensity is found on the ring.

It follows from Eqs. (28) and (29) that the intensity decreases from the maximum by e times in the points, which are located on a ring at the following angles from the intensity maximum:

$$\theta_e=\pm2\arcsin\left(\frac{1}{\sqrt{8n}}\sqrt{\sqrt{1+2n\frac{w_0^2}{D_0^2}}-1}\right).$$

This means that increasing of the asymmetry parameter leads to decreasing of the length of the arc of the light crescent. If $D_0\ll w_0$, then the intensity does not decrease e times on the whole ring. If $D_0\gg w_0$, then, vice versa, the intensity drops e times at $\theta_e\approx\pm w_0/(2^{1/2}D_0)$.

From Eqs. (28) and (29) it also follows that having traveled over a distance z, the maximum intensity drops by a factor of $1+(z/z_R)^2$.

In the initial coordinate system, the intensity maximum point has the coordinates

$$\begin{aligned}x_{\max}&=\mathrm{Re}x_0-\mathrm{Im}y_0\\ &\quad+\frac{(\mathrm{Im}x_0)z+(\mathrm{Im}y_0)z_R}{2z_R}\left(1+\sqrt{1+\frac{2nw_0^2}{D_0^2}}\right),\\ y_{\max}&=\mathrm{Re}y_0+\mathrm{Im}x_0\\ &\quad+\frac{(\mathrm{Im}y_0)z-(\mathrm{Im}x_0)z_R}{2z_R}\left(1+\sqrt{1+\frac{2nw_0^2}{D_0^2}}\right).\end{aligned} \tag{31}$$

From (31) it follows that the maximum intensity point $(x_{\max}, y_{\max})$ is rotating about the point $(x_{\min}, y_{\min})$, making an angle of α_0 at the distance

$$z=z_R\tan(\alpha_0). \tag{32}$$

Figure 4 shows transverse intensity patterns of the beam in Eq. (3) with zero radial index $m=0$ at different planes for the following parameters: wavelength $\lambda=532$ nm, waist radius $w_0=5\lambda$ (with the Rayleigh range equal to $z_R=25\pi\lambda$), the topological charge $n=8$, transverse shifts $x_0=0.25\lambda=w_0/20$ and $y_0=0.25i\lambda=iw_0/20$, on-axis

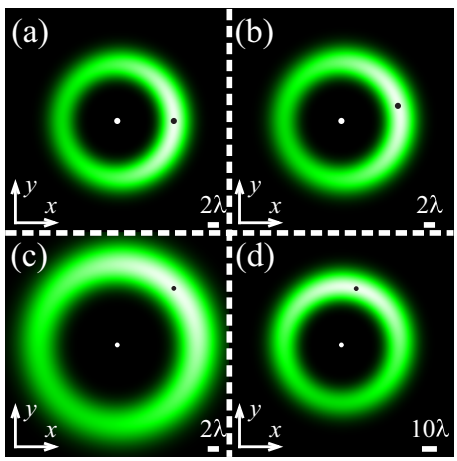

FIG. 4. Transverse intensity patterns of beam (3) with zero radial index $m=0$ at different distances for the following parameters: wavelength $\lambda=532$ nm, waist radius $w_0=5\lambda$, topological charge $n=8$, transverse shifts $x_0=0.25\lambda=w_0/20$ and $y_0=0.25i\lambda=iw_0/20$; the on-axis distances are $z=0$ (a), $z_R\tan(\pi/12)$ (b), $z_R\tan(\pi/4)=z_R$ (c), and $z_R\tan(5\pi/12)$ (d). The computational domain size is $2R$, where $R=20\lambda$ (a), 20λ (b), 20λ (c), and 75λ (d). The black dot shows the location of the intensity maximum derived from (31).

distances $z = 0$ [Fig. 4(a)], $z_R\tan(\pi/12)$ [Fig. 4(b)], $z_R\tan(\pi/4) = z_R$ [Fig. 4(c)], and $z_R\tan(5\pi/12)$ [Fig. 4(d)]. The beam center is at the origin of the coordinates: $(x_{\min}, y_{\min}) = (0, 0)$. The computational domain size is $2R$, where $R = 20\lambda$ [Fig. 4(a)], 20λ [Fig. 4(b)], 20λ [Fig. 4(c)], and 75λ [Fig. 4(d)]. The black dot marks the location of the intensity maximum, which was calculated using (31). The white dot marks the location of the minimal intensity or a phase singularity point.

From (28)–(30) it follows that the ratio of the maximal intensity on the diffraction ring to a minimal one (in the saddle point) is defined by the relation

$$\frac{I_{0n,\max}}{I_{0n,\text{saddle}}} = \left(\frac{\sqrt{D_0^2 + 2nw_0^2} + D_0}{\sqrt{D_0^2 + 2nw_0^2} - D_0}\right)^{2n} \times \exp\left(\frac{2D_0}{w_0^2}\sqrt{D_0^2 + 2nw_0^2}\right). \quad (33)$$

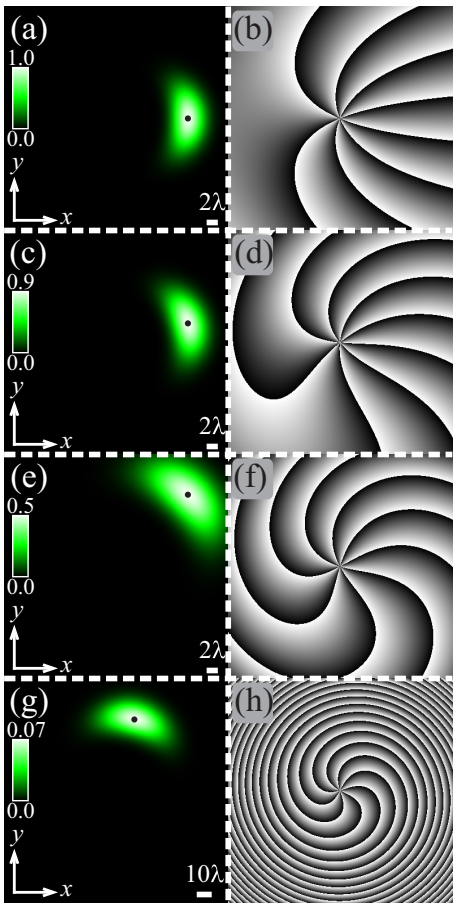

FIG. 5. Transverse intensity (a,c,e,g) and phase (b,d,f,h) patterns of beam (3) with zero radial index $m = 0$ at different distances z for the following parameters: wavelength $\lambda = 532\,\text{nm}$, waist radius $w_0 = 5\lambda$, topological charge $n = 8$, transverse shifts $x_0 = 5\lambda = w_0$ and $y_0 = 5i\lambda = iw_0$; on-axis distances are $z = 0$ (a, b), $z_R\tan(\pi/12)$ (c,d), $z_R\tan(\pi/4) = z_R$ (e,f), and $z_R\tan(5\pi/12)$ (g, h). The computational domain size is $2R$, where $R = 20\lambda$ (a–f), 75λ (g, h). The black dot marks the intensity maximum derived from (31). In the phase patterns black and white, respectively, mark $-\pi$ and $+\pi$.

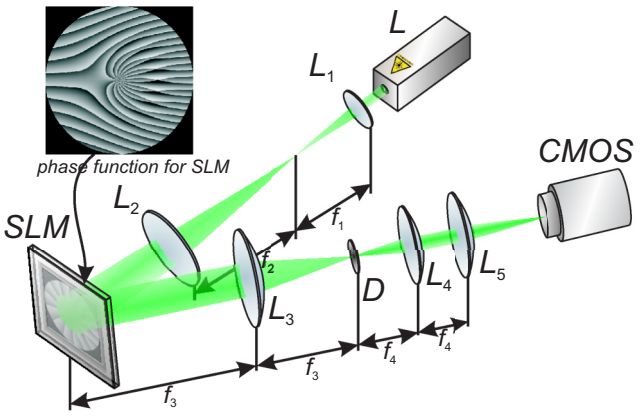

FIG. 6. Experimental setup for generating aLG beams: L is a solid-state laser ($\lambda = 532\,\text{nm}$); L_1, L_2, L_3, L_4, and L_5 are lenses with foci $f_1 = 250\,\text{mm}$, $f_2 = 500\,\text{mm}$, $f_3 = 350\,\text{mm}$, $f_4 = 150\,\text{mm}$, and $f_5 = 280\,\text{mm}$; SLM is a spatial light modulator PLUTO VIS (1920 × 1080 resolution and 8-μm pixels); D is a diaphragm serving as a spatial filter; CMOS is a video camera, LOMO TC-1000 (3664 × 2740 resolution and 1.67-μm pixels).

From (33), the asymmetry of the beam is seen to increase with increasing shift D_0. What this means is that with increasing imaginary shifts $\text{Im}(x_0)$ and $\text{Im}(y_0)$ a disintegration of the bright ring occurs, with the intensity pattern appearing as an off-center bright spot rotating upon propagation about a phase singularity point $(x_{\min}, y_{\min})$. The term "disintegration" is in quotation marks because the intensity nowhere becomes zero in the bright ring, as the denominator in (33) never turns zero at $n > 0$.

Figure 5 depicts the simulation results for the transverse intensity pattern and the phase of the same beam as was depicted in Fig. 4, but with larger shifts: $x_0 = 5\lambda = w_0$ and $y_0 = 5i\lambda = iw_0$. The rest of the parameters remained unchanged. The black dot marks the intensity maximum calculated from (31). Color bars confirm that upon propagation the intensity drops by a factor of $1 + (z/z_R)^2$.

From Fig. 5, an oblong focal spot is seen to be rotated by respective angles of $\pi/12$, $\pi/4$, and $5\pi/12$, whereas the phase singularity center remains at the origin of coordinates.

At $m = 0$, an aLG beam is similar to an asymmetric Bessel-Gaussian (aBG) beam [28]. Both beams have the same rotation velocity defined by (32). Note, however, that with an aBG beam being more difficult to define analytically, only relationships for the coordinates of intensity zeros were deduced in [28], whereas the coordinates of intensity maxima similar to (31) were not analytically derived. As distinct from a closed-form relation for the OAM of an aLG beam in Eq. (22), the OAM of an aBG beam is defined via modified Bessel functions series. Besides, the OAM of an aLG beam is quadratically dependent on the asymmetry parameter, whereas the OAM of an aBG beam is described by a near-linear function [28].

VI. EXPERIMENTAL GENERATION OF AN ASYMMETRIC LAGUERRE-GAUSSIAN BEAM USING A SPATIAL LIGHT MODULATOR

The experimental optical setup is shown in Fig. 6. The output beam of a solid-state laser $L(\lambda = 532\,\text{nm})$ was

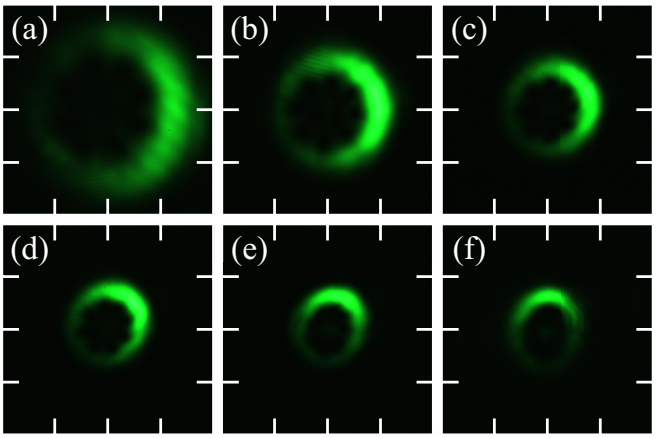

FIG. 7. Intensity patterns for an aLG beam, generated at different distances from the plane of lens L_5: (a) 0 mm, (b) 100 mm, (c) 150 mm, (d) 200 mm, (e) 250 mm, and (f) 280 mm. The scale size is 500 μm. Parameters are $w_0 = 1$ mm, $n = 8$, $x_0 = 0.2w_0$, and $y_0 = 0.2w_0 i$.

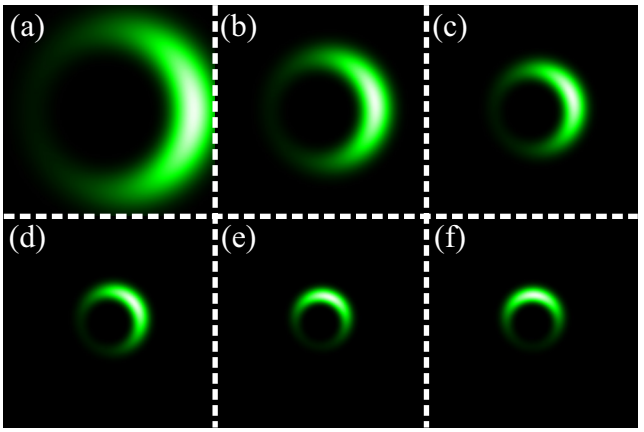

FIG. 8. Intensity patterns of an aLG beam calculated using Eq. (3) (with regard for the lenses) at the parameters used in Fig. 7.

expanded using a system composed of lenses $L_1(f_1 = 250\,\text{mm})$ and $L_2(f_2 = 500\,\text{mm})$. The expanded laser beam with radius of about 1.1 mm illuminated the display of a spatial light modulator (SLM) (PLUTO VIS, 1920 × 1080 resolution, with 8-μm pixels). The input of the SLM display was composed of a phase function generated by the superposition of the encoded phase function of the initial element used to generate the aLG beam and a linear phase mask (see inset in Fig. 6). The aim was to separate spatially the first and zero diffraction orders, with the nonmodulated wave being reflected to the latter. Using lenses $L_3(f_3 = 350\,\text{mm})$ and $L_4(f_4 = 150\,\text{mm})$, the laser beam reflected to the first order was guided to a lens $L_5(f_5 = 280\,\text{mm})$, which focused the aLG beam onto a complementary metal-oxide semiconductor (CMOS) array of the LOMO TC-1000 video camera (3664 × 2740 resolution, 1.67-μm pixels). The CMOS camera was mounted on an optical rail to travel along and register the intensity pattern at different distances from lens L_5. The diaphragm D served to filter out the zero diffraction order.

Figure 7 depicts the intensity patterns registered at different distances from the surface of lens L_5. While registering the pattern at distance 0 mm, the lens L_5 was temporarily removed from the setup. The depicted images show that the crescent-shaped beam rotate about the axis with increasing distance from the lens. The beam generated in the focus of lens L_5 is seen to be rotated by 90° with respect to that in the plane of lens L_5. In addition, due to focusing, the transverse size of the beams is also reduced.

Figure 8 shows the intensity patterns calculated using Eq. (3), with regard for the lenses, at the parameters of the experiment. From Fig. 8, the experimental and calculated patterns are seen to be in qualitative agreement.

VII. ROTATING SUPERPOSITIONS OF ASYMMETRIC LAGUERRE-GAUSSIAN BEAMS

As the imaginary shifts x_0 and y_0 further increase, the beam's asymmetry increases to the extent that the intensity on the ring gets concentrated near a maximum point, defined by (31). Rather than being a crescent, the intensity pattern looks more like a Gaussian beam, which is shifted from the origin and rotated by an angle of $\pi/2$ upon propagation.

Actually, according to Eq. (28), in the initial plane of the rotated coordinate system (26), the intensity is distributed by the law

$$I_{0n}(\xi,\eta,z=0) = \left(\frac{\sqrt{2}}{w_0^2}\right)^n \exp\left(\frac{2D_0^2}{w_0^2}\right)(\xi^2+\eta^2)^n \times \exp\left\{-\frac{2}{w_0^2}[(\xi - D_0)^2 + \eta^2]\right\}. \quad (34)$$

In the other planes at distance z, the intensity in Eq. (34) takes the form

$$I_{0n}(\xi,\eta,z) = \frac{w^2(0)}{w^2(z)}\left[\frac{\sqrt{2}}{w^2(z)}\right]^n \exp\left(\frac{2D_0^2}{w_0^2}\right)(\xi^2+\eta^2)^n \times \exp\left(-\frac{2}{w^2(z)}\{[\xi - D(z)]^2 + \eta^2\}\right), \quad (35)$$

where $D(z)/D_0 = [1 + (z/z_R)^2]^{1/2} = w(z)/w(0)$.

That is, at $D_0 \gg w_0$ the power component $(\xi^2+\eta^2)^n$ weakly affects the intensity pattern, with the remaining exponential component in (35) corresponding to the intensity pattern of a Gaussian beam with waist radius $w(z)$, shifted by distance $D(z) \approx \xi_{\max}$ from the origin (where the phase singularity is found). Hence, the superposition of beams (34) with different shifts D_0 will appear as misaligned Gaussian beams, which are rotated by the same angle defined by (32) as they propagate. Also, note that according to (35), with increasing distance z from the initial plane, there will be a $[1 + (z/z_R)^2]^{1/2}$ times increase in the off-axis shift of the intensity maxima, which is proportional to the Gaussian beam expansion. What this means is that as they propagate, the beams hardly interfere with each other and the diffraction pattern remains unchanged.

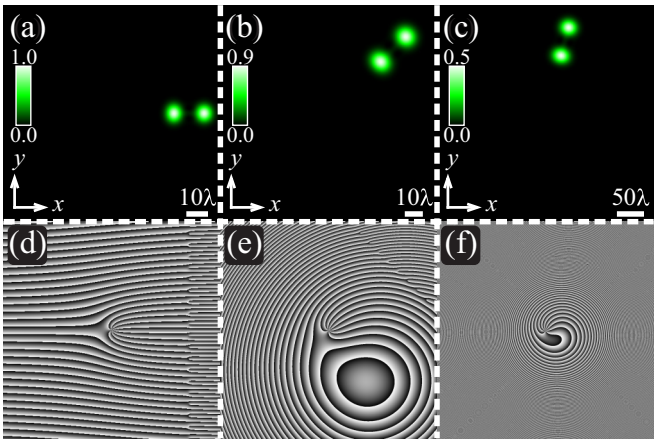

FIG. 9. Intensity (a–c) and phase (d–f) patterns of the aLG beams (36) at the parameters ($N = 2$): wavelength $\lambda = 532$ nm, waist radius $w_0 = 5\lambda$, beam index $(m, n) = (0, 8)$; the transverse shifts $x_0 = 5w_0$, $y_0 = 5w_0 i$ (for the first beam) and $x_0 = 8w_0$, $y_0 = 8w_0 i$ (the second beam); the on-axis distances $z = 0$ (a,d), $z = z_R \tan(\pi/4)$ (b,e), and $z = z_R \tan(5\pi/12)$ (c,f). The computational domain size is $2R$, where $R = 50\,\lambda$ (a,d), 60λ (b,e), and 200λ (c,f). In the phase patterns, black and white, respectively, mark $-\pi$ and $+\pi$.

Figure 9 illustrates the propagation of two aLG beams, with their complex amplitude given by

$$E(x,y,z) = \frac{w(0)}{w(z)}\left[\frac{\sqrt{2}}{w(z)}\right]^n \times \sum_{j=1}^{N} C_j[(x - x_{0j}) + i(y - y_{0j})]^n \times \exp\left[-\frac{s_j^2}{w^2(z)} + \frac{iks_j^2}{2R(z)} - i(n+1)\zeta(z)\right], \quad (36)$$

where $N = 2$ for two beams, (x_{0j}, y_{0j}) are the shifts of the jth beam, and $s_j = [(x-x_{0j})^2 + (y-y_{0j})^2]^{1/2}$. The C_j coefficients were fitted so as to attain the same maximum intensity for all constituent beams. The rest of the parameters of the simulation were as follows: $\lambda = 532$ nm; waist radius $w_0 = 5\lambda$ (Rayleigh range $z_R = 25\pi\lambda$); beam index $(m, n) = (0, 8)$; the transverse shifts of the first beam, $x_0 = 5w_0$, $y_0 = 5w_0 i$, of the second beam, $x_0 = 8w_0$, $y_0 = 8w_0 i$; the on-axis distances, $z = 0$ [Figs. 9(a) and 9(d)], $z = z_R \tan(\pi/4)$ [Figs. 9(b) and 9(e)], and $z = z_R \tan(5\pi/12)$ [Figs. 9(c) and 9(f)]. The computational domain size was $2R$, where $R = 50\lambda$ [Figs. 9(a) and 9(d)], 60λ [Figs. 9(b) and 9(e)], and 200λ [Figs. 9(c) and 9(f)].

From Fig. 9, the beam similar to the superposition of two Gaussian beams is seen to remain nearly unchanged upon propagation (within a scale), being rotated by an angle of $\pi/4$ [Figs. 9(b) and 9(e)] and $5\pi/12$ [Figs. 9(c) and 9(f)].

VIII. CONCLUSION

Summing up, we have proposed a generalization of well-studied Laguerre-Gaussian modes. Asymmetric Laguerre-Gaussian beams have no modal properties, showing an asymmetric intensity pattern in a plane perpendicular to the propagation axis. As an asymmetric LG beam propagates in a uniform space, the asymmetry of the first diffraction ring decreases, with the energy being redistributed to peripheral rings. The number of diffraction rings is coincident with that of a conventional (symmetric) LG beam. The power transferred by aLG beams and the projection of their OAM onto the optical axis have been analytically derived. The normalized OAM has been found to increase quadratically with increasing asymmetry parameter, which is defined as the ratio of the Cartesian shift to the Gaussian beam radius. Conditions for the normalized OAM becoming equal to the topological charge (as is the case for conventional LG beams) have been derived. A particular case of the aLG beams with zero radial index that have a crescent-shaped transverse intensity pattern has been discussed. A relation to describe the coordinate of the intensity maximum has been deduced and the intensity crescent has been shown to rotate during propagation in space. An aLG beam with zero radial index has been generated using a liquid-crystal SLM. The crescent-shaped transverse intensity pattern has been experimentally shown to rotate upon propagation. A feasibility to generate misaligned superpositions of aLG beams with a near-Gaussian intensity distribution that rotate as a whole upon propagation has been demonstrated. The crescent-shaped aLG beams can find uses for trapping and manipulating biological objects (cells) [29], because in this case the cell is less exposed to heat than compared with traps based on a symmetric Gaussian beam. The aLG beams will also be useful in quantum communications systems to form the entanglement of the OAM states of photons. Considering that the aLG beams can carry both integer and fractional OAM, the latter corresponds to the entanglement of the OAM state of a photon [30]. That is, if the aLG-beam is used as a pumping laser beam in the spontaneous parametric downconversion, two photons should appear with the entangled OAM.

Note that any solution of the paraxial equation can be shifted by complex distances along the Cartesian coordinates. This leads to a new solution. Therefore, it would be interesting to study other beams in the same way: asymmetric Hermite-Gaussian [31], asymmetric Ince-Gaussian [23], and the like.

ACKNOWLEDGMENTS

The work was partially funded by the Russian Federation Ministry of Education and Science, Russian Federation President's grants for support of leading scientific schools (Grant No. NSh-9498.2016.9), and Russian Foundation for Basic Research Grants No. 14-29-07133, No. 15-07-01174, No. 15-37-20723, No. 15-47-02492, and No. 16-29-11698.

[1] S. Huang, Z. Miao, C. He, F. Pang, Y. Li, and T. Wang, Opt. Lasers Eng. **78**, 132 (2016).
[2] W. N. Plick and M. Krenn, Phys. Rev. A **92**, 063841 (2015).
[3] D. A. Savelyev and S. N. Khonina, Comput. Opt. **39**, 654 (2015).

[4] A. B. Stilgoe, T. A. Nieminen, and H. Rubinsztein-Dunlop, J. Opt. **17**, 125601 (2015).
[5] Y. Zhang, X. Liu, M. Belić, W. Zhong, F. Wen, and Y. Zhang, Opt. Lett. **40**, 3786 (2015).
[6] D. J. Kim and J. W. Kim, Appl. Phys. B **121**, 401 (2015).
[7] D. Lin, J. Daniel, and W. Clarkson, Opt. Lett. **39**, 3903 (2014).
[8] G. Ruffato, M. Massari, and F. Romanato, Opt. Lett. **39**, 5094 (2014).
[9] E. Karimi, R. W. Boyd, P. de la Hoz, H. de Guise, J. Rehacek, Z. Hradil, A. Aiello, G. Leuchs, and L. L. Sanchez-Soto, Phys. Rev. A **89**, 063813 (2014).
[10] B. C. Das, D. Bhattacharyya, and S. De, Chem. Phys. Lett. **644**, 212 (2016).
[11] A. Allocca, A. Gatto, M. Tacca, R. A. Day, M. Barsuglia, G. Pillant, C. Buy, and G. Vajente, Phys. Rev. D **92**, 102002 (2015).
[12] K. Sun, C. Qu, and C. Zhang, Phys. Rev. A **91**, 063627 (2015).
[13] P. K. Mondal, B. Deb, and S. Majumder, Phys. Rev. A **89**, 063418 (2014).
[14] T. Otsu, T. Ando, Y. Takiguchi, Y. Ohtake, H. Toyoda, and H. Itoh, Sci. Rep. **4**, 4579 (2014).
[15] M. Krenn, R. Fickler, M. Fink, J. Handsteiner, M. Malik, T. Scheidl, R. Ursin, and A. Zeilinger, New J. Phys. **16**, 113028 (2014).
[16] M. Krenn, J. Handsteiner, M. Fink, R. Fickler, and A. Zeilinger, Proc. Natl. Acad. Sci. USA **112**, 14197 (2015).
[17] V. Grillo, G. C. Gazzadi, E. Mafakheri, S. Frabboni, E. Karimi, and R. W. Boyd, Phys. Rev. Lett. **114**, 034801 (2015).
[18] C. W. Clark, R. Barankov, M. G. Huber, M. Arif, D. Cory, and D. A. Pushin, Nature **525**, 504 (2015).
[19] Yu. A. Kravtsov, Radiophys. Quantum Electron. **10**, 719 (1967).
[20] V. V. Kotlyar, A. A. Kovalev, and V. A. Soifer, Opt. Lett. **39**, 2395 (2014).
[21] M. A. Bandres and J. C. Gutierrez-Vega, Opt. Express **16**, 21087 (2008).
[22] M. A. Bandres and J. C. Gutierrez-Vega, Opt. Lett. **33**, 177 (2008).
[23] M. A. Bandres, Opt. Lett. **29**, 1724 (2004).
[24] H. C. Kim and Y. H. Lee, Opt. Commun. **169**, 9 (1999).
[25] I. S. Gradshteyn and I. M. Ryzhik, *Table of Integrals, Series, and Products* (Academic, New York, 1965).
[26] A. P. Prudnikov, Y. A. Brychkov, and O. I. Marichev, *Integrals and Series: Special Functions* (Gordon & Breach, New York, 1986).
[27] A. A. Kovalev, V. V. Kotlyar, and A. P. Porfirev, Phys. Rev. A **91**, 053840 (2015).
[28] V. V. Kotlyar, A. A. Kovalev, R. V. Skidanov, and V. A. Soifer, J. Opt. Soc. Am. A **31**, 1977 (2014).
[29] M. A. Rykov and R. V. Skidanov, Appl. Opt. **53**, 156 (2014).
[30] A. Mair, A. Vaziri, G. Weihs, and A. Zeilinger, Nature **412**, 313 (2001).
[31] V. V. Kotlyar and A. A. Kovalev, J. Opt. Soc. Am. A **31**, 274 (2014).